Topology optimization of piezo modal transducers with null-polarity phases

Donoso, A.; Sigmund, O.

Published in:
Structural and Multidisciplinary Optimization

Link to article, DOI:
10.1007/s00158-015-1330-0

Publication date:
2016

Document Version
Peer reviewed version

Structural and Multidisciplinary Optimization manuscript No.
(will be inserted by the editor)

Topology optimization of piezo modal transducers with null-polarity phases

A. Donoso · O. Sigmund

Received: date / Accepted: date

Abstract Piezo modal transducers in 2d can be designed theoretically by tailoring polarity of the surface electrodes. However, it is also necessary to include null-polarity phases of known width separating areas of opposite polarity in the manufacturing process in order to avoid short-circuiting. Otherwise the performance of such devices could be spoiled. In this work, we propose an appropriate topology optimization interpolation function for the electrode profile such that the effect of this new phase (hereafter gap-phase) is included in the formulation of the design problem. The approach is density-based, where the interface is controlled by including the gradient norm in the electrode profile interpolation. Through a detailed case study in 1d, conclusions on how to control the width of this gap-phase are extracted, and subsequently extended to the 2d case.

Keywords Topology optimization · Piezoelectric effect · Modal filters · Gap-phase · Two-step filtering

The major part of this research was performed while A. Donoso was a visiting researcher at the Department of Mechanical Engineering, Technical University of Denmark, during August 2014.

A. Donoso (Corresponding Author)
Departamento de Matemáticas, ETSII
Universidad de Castilla - La Mancha
13071 Ciudad Real, (Spain)
E-mail: Alberto.Donoso@uclm.es

O. Sigmund
Department of Mechanical Engineering
Section of Solid Mechanics
Technical University of Denmark
Nils Koppels Alle, Building 404
DK-2800, Kgs. Lyngby (Denmark)
E-mail: sigmund@mek.dtu.dk

1 Introduction to piezo modal transducers

Piezo modal sensors/actuators are those piezoelectric transducers which measure/excite a specific eigenmode of a structure, but also remain insensitive to the rest i.e., they behave as spatial filters (also called modal filters) in the frequency domain (Lee and Moon 1990).

A typical configuration of a piezoelectric transducer is shown in Fig. 1(left). It is formed by the host structure with a piezoelectric layer bonded to its upper surface. As the piezo material is dielectric, two electrodes on both sides of the piezo are required to collect the charge generated as sensor to an external measurement device. If the electrode now is shaped in an appropriate way as Fig. 1 (right) shows (same pattern on both sides of the piezo layer), then we could get the effect desired, that is, the transducer isolates a single mode of a structure from the rest. Therefore, to design modal transducers we have to determine which regions of the piezo layer have to be covered by an electrode and decide their polarity, and which ones are not.

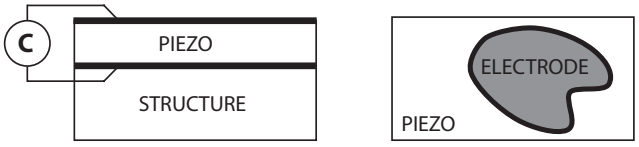

Fig. 1 Schematic diagram of a piezoelectric transducer; (left) cross section of a structure with a piezo layer surface bonded; (right) top view of the surface electrode.

In the pioneering work by Lee and Moon (1990), the problem of designing modal transducers for beam-type structures is elegantly solved due to the fact that the mode shapes of those structures are orthogonal to each other with respect to the unit weight function. In such

cases the solution is confined to computing the surface electrode width only, according to the curvature of the mode of interest. Moreover, the authors prove that the pair modal sensor/actuator which measures/excites the same mode shape presents the same pattern thanks to the reciprocity of the piezoelectric effect.

Unfortunately, this approach cannot be extended to the 2d case for different reasons. To this purpose, many authors have studied the underlined problem in detail and just some of them are mentioned here. In Kim et al. (2001), though the results obtained are satisfactory, the way to implement the topologies obtained requires extra interface circuits and complicates electrode patterns over rough meshes resulting from genetic algorithms. Sun et al. (2002) proposed structures composed of many small piezo patches of different and uniform thickness. Preumont et al. (2005) introduced a new porous distributed electrode concept. In Jian and Friswell (2007), the shape of a sensor is optimized. Although the polarization profile is also initially considered in the model, it is not used in the optimization process as a design variable any more. More recently, electrode-shaping techniques have been performed in Pulskamp et al. (2012) to detect modes only, but not to cancel others. Also Zhang et al. (2014) reduce the sound radiation in shells under harmonic excitations.

On the other hand, since the work of Silva and Kikuchi (1999), where in-plane piezoelectric resonators are designed, the number of papers related to the design of piezo transducers by using topology optimization is really overwhelming. We cite here some of them. Kögl and Silva (2005) considered the optimization of the piezoelectric layers together with the polarization profile for statics. Carbonari et al. (2007) and Luo et al. (2010), among others, optimized both the host structure and the piezo layers to design in-plane multi-phase actuators. More recently, Kang et. al (2012) have gone further, on including as a third design variable the spatial distribution of the control voltage in the optimization problem, in some way connected with the polarity of the piezoelectric layers.

In line with the ideas of Jian and Friswell (2007) and using the philosophy of topology optimization (the reader is referred to Bendsøe and Sigmund 2003 for an overview of the method and different applications), we emphasize the technique described in Donoso and Bellido (2009a). In that work, a systematic procedure to design piezoelectric modal transducers for plate-type structures of arbitrary dimensions $L_x \times L_y$ was developed.

In the present study, we assume that the piezoelectric layer has a negligible thickness compared to the one of the plate as illustrated in Fig. 2(a). This assumption is very common, especially when working at the micro scale as we do here. The design scheme for ensuring finite size electrode gaps suggested in this paper, however, is general and can just as well be used for cases where the ratio between the thickness of the plate and the piezo is large. The only difference is the modeling part which becomes more complicated. Moreover, we consider same piezoelectric constants in both spatial directions, x, y, and piezo axes coincident with the geometric ones of the plates, as in e.g. hexagonal class 6 mm crystals. Based on these assumptions, it is important to notice that the piezoelectric properties are not needed in the problem formulation and just appear as a scaling factor that we will omit for the sake of simplicity. Again, however, including anisotropic piezoelectric properties will only change the modeling complexity and not the proposed gap-phase scheme.

Looking back to the underlying work, we remark the two main contributions: first, regarding the problem of designing a modal transducer that isolates the kth mode from the first M modes as the optimization problem

$$\max_{\chi} : F_k(\chi) \tag{1}$$

subject to

$$F_j(\chi) = 0, \quad j = 1, \cdots, M, \;\; j \neq k \tag{2}$$

where the mode sensitivity of the jth mode

$$F_j = \int_0^{L_y} \int_0^{L_x} P(x,y) \left(\frac{\partial^2 \phi_j}{\partial x^2} + \frac{\partial^2 \phi_j}{\partial y^2} \right) \, dx \, dy \tag{3}$$

is connected with its corresponding mode shape ϕ_j only. P is the polarity of the electrode (Fig. 2(b)) given by

$$P(x,y) = 2\chi(x,y) - 1, \tag{4}$$

with the design variable χ controlling the electrode profile such that $\chi \in \{0, 1/2, 1\}$ (negative, null or positive polarity); and second, proving analytically that such an optimization problem admits optimal solutions (rather than optimized ones) with polarity taking exclusively -1 or 1 values. Since the optimized polarity never takes value 0, this means that the host structure is covered throughout by an electrode in the optimum, as we can see in Fig. 2(c) (notice that they are really pure 0-1 designs). Therefore, the discrete problem can efficiently be solved by using the simplex method, without requiring filters nor projection or penalization methods (Guest et al. 2004, Sigmund 2007).

Above mentioned approach, initially formulated for the out-of-plane case, was generalized to the in-plane case (Donoso and Bellido 2009b) and to shells (Donoso et. al 2010). After that, our work continued by designing micro transducers that were manufactured and tested

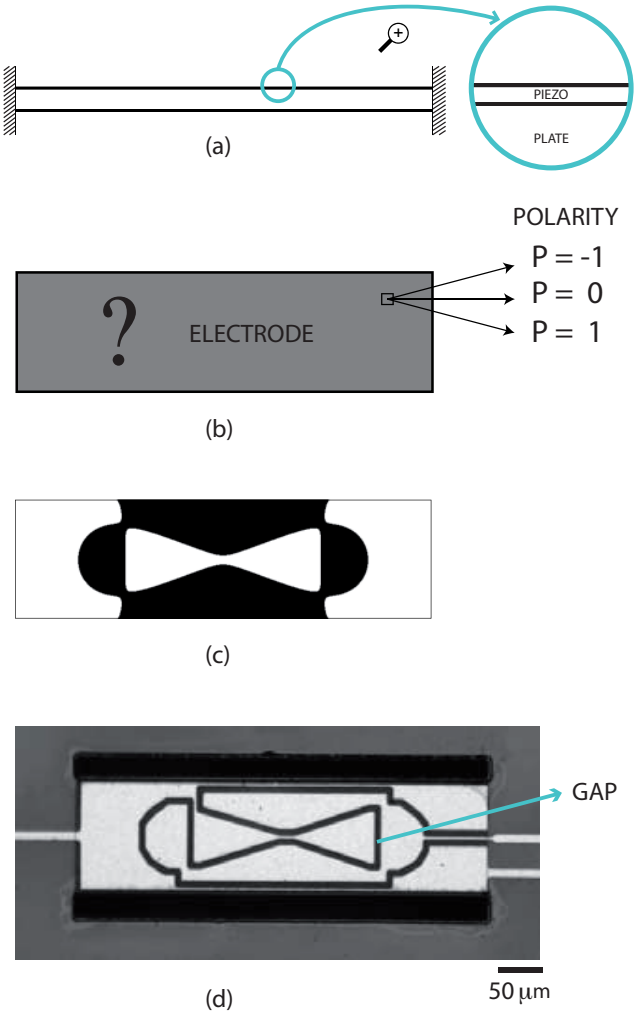

Fig. 2 (a) Side view of a micro plate of 680 μm in length and 200 μm in width clamped at its both extreme sides; (b) Top view of the design domain (electrode); (c) Electrode profile that isolates the first mode from the first 14 out-of-plane modes. Black and white phases denote regions with opposite polarity; (d) Manufactured design with a gap-phase of width $w_{gap} = 5$ μm. This example has been extracted from Sánchez-Rojas et al. (2010).

showing quite good performance in general (Sánchez-Rojas et al. 2010). However, we could check that part of the discrepancies between the tested filters and the ideal ones come from the fabrication. The problem was that in the lithography process (the different steps are described in detail in Kucera et al. 2013) a uniform null-polarity phase (gap-phase) corresponding to $\chi = 1/2$ (or equivalently $P = 0$) of a few microns was required (for structures of some hundreds of microns size) between areas of opposite polarity in order to avoid short-circuiting in the manufactured structures (see Fig. 2(d)).

To go into more detail, the (theoretical) optimized designs obtained through our approach are very sensitive to the width of the gap-phase, even before having manufactured them. This fact is highlighted in Fig. 3, where the mode sensitivities corresponding to the example shown in Fig. 2(c) are represented for different width values of the gap-phase. It is observed how some mode coefficients rise with the introduction of a gap-phase. Clearly, that makes us conclude that the gap-phase must be included in the problem formulation rather than imposing it over the optimal structure at a later stage. It seems obvious that the sensitivity to a gap-phase strongly depends on the scale of the device, and for a micro device, as in our case, the width of the gap is much more critical than for a macro structure. It is important to notice that this issue should be taken into account not only for designing piezo modal transducers, but also piezo transducers in general presenting regions with opposite polarities in contact.

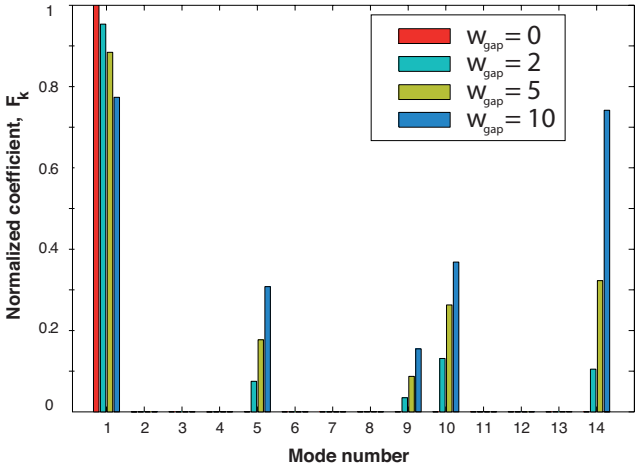

Fig. 3 Mode sensitivity in Fig. 2(c) when a gap-phase of width 0 μm, 2 μm, 5 μm and 10 μm is imposed a posteriori.

In order to enforce a new material-phase between two given phases we use the scheme recently suggested by Clausen et al. (2015). In this research, a coating material (which plays the role of the gap-phase in our problem) is enforced in a base structure made from a porous material and void.

In this paper, inspired by the aforementioned work, we reconsider the problem of designing piezoelectric transducers that isolate a specific mode and suppress as much as possible the response of the other modes (among the first M modes), but include the requirement that a gap-phase of given width must separate areas of positive and negative polarity.

The layout of the paper is as follows. Section 2 is devoted to the interpolation scheme proposed for the electrode profile ensuring a gap-phase. Also a didactic example in 1d is included to understand how we can control the width of the gap. In Section 3, an alterna-

tive formulation for solving the general problem is proposed together with the sensitivity analysis. Section 4 is dedicated to numerical examples in 2d. Finally, some conclusions are discussed in the last section.

2 On how to include a gap-phase

The aim of this section is to find an interpolation function for the polarity that ensures a gap-phase between regions with opposite polarizations. As this phase is enforced at the interface of areas of opposite polarities where the gradient norm of the design field is high (theoretically infinite), the new interpolation function has to incorporate a filtered underlying gradient norm.

2.1 Interpolation function

Inspired by the work of Clausen et al. (2015), the new interpolation function proposed for the electrode profile is the following

$$P(\varphi, \overline{\|\nabla\hat{\varphi}\|_\delta}) = (2\varphi - 1)(1 - \overline{\|\nabla\hat{\varphi}\|_\delta}), \quad \varphi \in [0,1] \tag{5}$$

where φ (the only independent field as it will be shown later) is the filtered (smoothed and projected) design field. More specifically, to understand how it works, first we consider the usual design field called here $\rho \in [0,1]$. The term $(2\rho - 1)$ takes values between -1 and 1. This field, ρ, is smoothed (giving $\hat{\rho}$) and projected (giving $\overline{\hat{\rho}} \equiv \varphi$), arriving at the term $(2\varphi - 1)$. This first-step filtering provides the areas with opposite polarity, that is, both black and white phases.

In order to identify correctly the interface between them, a second-step filtering is necessary. It starts by smoothing φ (giving $\hat{\varphi}$). It is the norm of the spatial gradient of this field smoothed $\|\nabla\hat{\varphi}\|$ the one which roughly defines the interface. Since this norm typically is small, it is necessary to scale it so that the maximum values are close to one (we show later how to obtain the value of the scaling factor δ). Finally, the scaled or normalized norm $\|\nabla\hat{\varphi}\|_\delta$ is projected again to model a sharp interface, and precisely this second field $\overline{\|\nabla\hat{\varphi}\|_\delta}$ defines the gap-phase. Hence, the new interpolation function for the electrode profile verifies on the one hand that $P(0,0) = -1$ and $P(1,0) = 1$. This means that inside black and white regions, the second field is null and the polarity would be negative or positive, respectively. On the other hand, the gap-phase is enforced when the second field equals 1, that is, $P(\varphi, 1) = 0$.

One could consider other tentative "second" fields such as $\overline{\|\nabla\hat{\rho}\|_\delta}$ or $\overline{\|\nabla\varphi\|_\delta}$, but none of them work well in our experience. In the former case the interface is not well detected because the gradients are not crisp enough, and in the latter a mesh-dependence effect is observed when making the projection sharper.

In the next subsection, we will illustrate by a 1d example how the two phases appearing in our problem are properly separated by using the two-step filtering process.

2.2 An example of two-step filtering in 1d

Let us consider a beam of length L clamped at both extremes (see Fig. 4(a)) for which we are interested in maximizing the first-mode sensitivity including a gap-phase wherever needed. The discrete formulation would be

$$\max_{\boldsymbol{\rho}} : F_1(\boldsymbol{\rho}) \equiv \mathbf{G}_1^T \mathbf{P}(\boldsymbol{\rho}) \tag{6}$$

subject to

$$0 \leq \rho_e \leq 1, \quad e = 1, \cdots, N_e \tag{7}$$

where $\mathbf{G}_1$ is the term concerning the strains in the 1st mode, $\mathbf{P}$ is the discrete profile, and N_e is the number of elements in the discretization. The optimal solution without considering gap-phase is given in Fig. 4(b), where it is clearly observed how the interfaces (just two points) physically take place where there is a sign change in the curvature.

Now we would like to place a gap-phase of known width, w_{gap}. To this purpose, we start considering the design field ρ. Then we obtain the smoothed field $\hat{\rho}$ as a solution to the PDE-filter - an ODE in 1d (Lazarov and Sigmund 2011)

$$-r_1^2 \hat{\rho}'' + \hat{\rho} = \rho \tag{8}$$

with Neumann boundary conditions, that is, $\hat{\rho}'(0) = \hat{\rho}'(L) = 0$ (the effect of using different boundary conditions will be discussed in the next subsection). The usual filter radius now called R_1 is expressed as $R_1 = 2\sqrt{3}r_1$. Notice that the ODE is solved for the nodal density variables, so FE discretization leads to the following system of linear equations (Andreassen et al. 2011)

$$\mathbf{K_{F_1}} \hat{\boldsymbol{\rho}}_{\boldsymbol{N}} = \mathbf{T_F} \boldsymbol{\rho} \tag{9}$$

where $\mathbf{K_{F_1}}$ is the standard FE stiffness matrix for scalar problems, $\mathbf{T_F}$ is a matrix which maps the element design values $\boldsymbol{\rho}$ to a vector with nodal values, and $\hat{\boldsymbol{\rho}}_{\boldsymbol{N}}$ is the nodal representation of the smoothed field. The one we are looking for is just

$$\hat{\boldsymbol{\rho}} = \mathbf{T_F}^T \hat{\boldsymbol{\rho}}_{\boldsymbol{N}} \tag{10}$$

The PDE-filter is preferred compared to the standard linear since field gradients are immediately available from its finite element discretization.

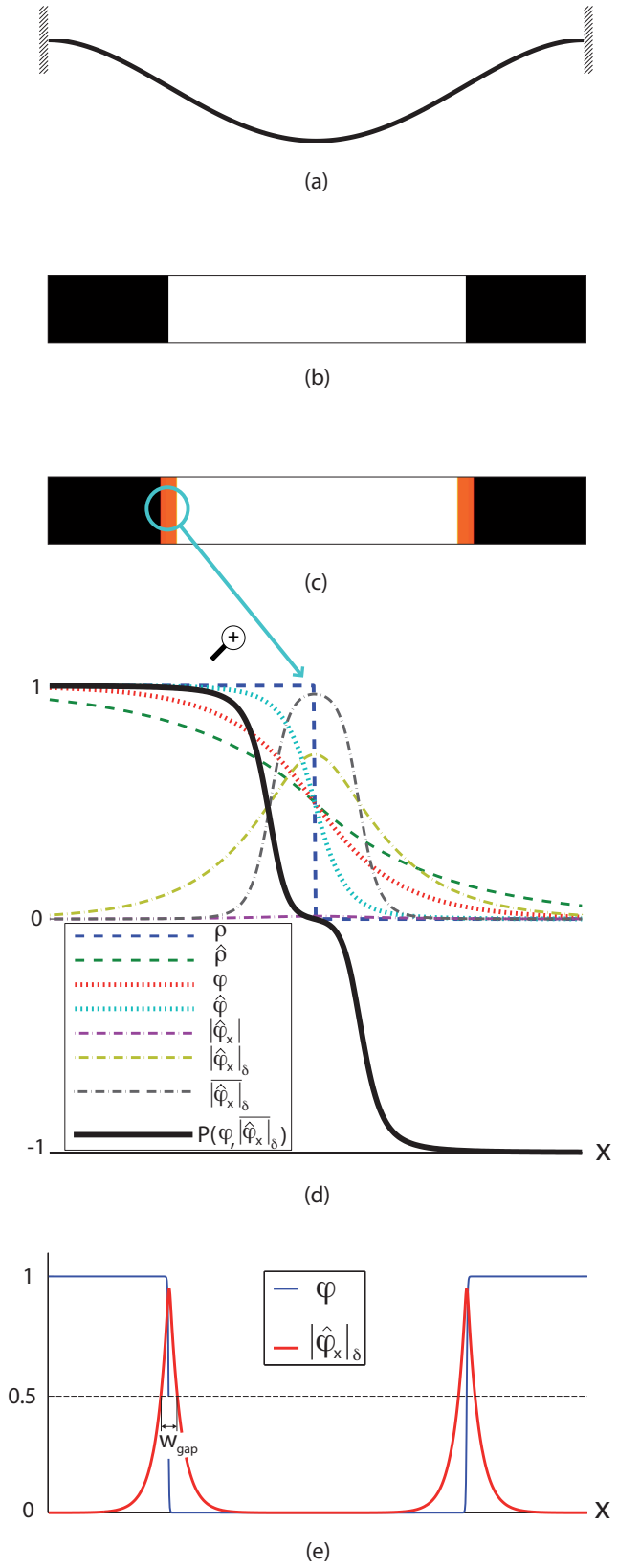

Fig. 4 (a) First mode of a clamped-clamped beam of L length; (b) Electrode profile that maximizes this shape, where black and white phases mean regions with opposite polarity; (c) The same on including a gap-phase of width $w_{gap} = 0.03L$ in each interface; (d) Interpolation function for the electrode profile with underlying two-step filtered fields; (e) On how the gap width is derived.

Finally, to ensure black-and-white designs, projection is performed using the smoothed Heaviside function proposed in Wang et al. (2011)

$$\varphi_e = \frac{\tanh(\beta_1\eta_1) + \tanh(\beta_1(\hat{\rho}_e - \eta_1))}{\tanh(\beta_1\eta_1) + \tanh(\beta_1(1-\eta_1))}, \quad \forall e \tag{11}$$

where β_1 determines the sharpness of the projection and $\eta_1 \in [0,1]$ is the threshold parameter. Up to this point, black and white phases meaning areas with opposite polarity are well defined.

Whenever β_1 is too high, the spatial gradient of the projected field, $\nabla\varphi$, is not well defined at sharp edges, so a new filtering process (with another filter radius R_2) is required where now φ plays the role of ρ before with identical boundary conditions, that is

$$\mathbf{K_{F_2}}\hat{\boldsymbol{\varphi}}_{\boldsymbol{N}} = \mathbf{T_F}\boldsymbol{\varphi} \tag{12}$$

Now the spatial gradient is directly computed by means of

$$\nabla\hat{\boldsymbol{\varphi}} \equiv |\hat{\boldsymbol{\varphi}}_x| = \mathbf{B}_x^T\hat{\boldsymbol{\varphi}}_{\boldsymbol{N}} \tag{13}$$

where $\mathbf{B}_x$ is the usual FE strain-displacement matrix. As commented before, the norm of this gradient $\|\nabla\hat{\boldsymbol{\varphi}}\|$ in the interface may be small, so basically we have to divide it by a scaling factor δ that upper bounds the norm to unity. In this case, the maximum value is obtained where φ has a discrete step edge, corresponding to the value $\delta = R_2/\sqrt{3}$ reported in Clausen et al. (2015). Finally, this field is again projected by choosing new values for the parameters β_2 and η_2, i.e.

$$\overline{\|\nabla\hat{\varphi}_e\|_\delta} = \frac{\tanh(\beta_2\eta_2) + \tanh(\beta_2(\|\nabla\hat{\varphi}_e\|_\delta - \eta_2))}{\tanh(\beta_2\eta_2) + \tanh(\beta_2(1-\eta_2))} \tag{14}$$

Assuming projection threshold parameters $\eta_2 = \eta_1 = 0.5$ and both β_2 and β_1 high enough values, then the projected fields have sharp edges. Under these assumptions, the gap width, w_{gap}, would be the distance between the two horizontal points that verify $\|\nabla\hat{\varphi}\|_\delta = \eta_2$, as shown in Fig. 4(e). By using a symbolic computation software an expression that upper bounds the gap width (the same as Clausen et al. 2015 derived from the coating problem) is obtained: the maximum value of the width converges quickly to a value which only depends on the second filter radius R_2,

$$w_{gap}^{max} = \frac{\ln(2)}{\sqrt{3}}R_2 \approx 0.4R_2 \tag{15}$$

We have tested this idea for different mesh sizes with fixed R_2 value, as well as varying R_2 for a fixed mesh. For our example, using a beam of length 1000 with unit element side length ($N_e = 1000$), $R_1 = 100$ (corresponding to a filter size of 100 elements in the first step) and $R_2 = 75$ (corresponding to a filter size of 75 elements in the second step), a gap of width $w_{gap} = 30$

(30 elements of unit length) is obtained in both sides, as we can see in Fig. 4(c). In such a case, the polarization profile, P, depicted with the rest of variables in Fig. 4(d) after the first iteration tends to take three values only, -1 (white-phase), 0 (gap-phase), 1 (black-phase).

2.3 On how to impose a gap-phase on the boundary

Owing to manufacturing reasons, it is advisable to impose an outside frame of gap-phase in the designs, typically of the same width as the one imposed inside. If we apply Dirichlet boundary conditions to the filter by means of $\hat{\rho}(0) = \hat{\rho}(L) = 1/2$, then a gap-phase of half width appears naturally on the boundary (just half of the design is shown in Fig. 5(b) due to symmetry reasons). So we can get a gap-phase of the same width of that imposed in the interior just using the previous boundary conditions and at the same time defining a passive area along the domain boundaries with half of the gap width. Now we should have in mind that nodes inside the passive area are excluded from the filter, and nodes at the interface between the passive area and the active part of the domain are restricted to $\hat{\rho} = 1/2$.

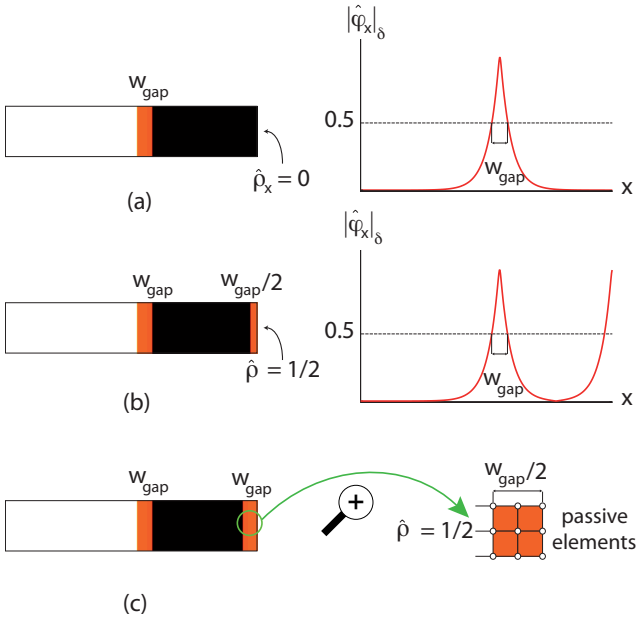

Fig. 5 (a) Half electrode profile of the previous example on using null Neumann boundary conditions; (b) Same with Dirichlet boundary conditions; (c) Same with Dirichlet boundary conditions and a passive area.

3 Problem formulation

Now we are interested in finding a modal sensor that filters the kth mode among the first M modes, and suppress as much as possible the rest of them. Notice that on introducing the gap-phase, the condition of ideal filter $F_j = 0$ will probably not be attainable any more, so we consider the following formulation instead

$$\max_{\boldsymbol{\rho}} : F_k(\boldsymbol{\rho}) \tag{16}$$

subject to

$$\begin{array}{ll} |F_j(\boldsymbol{\rho})| \leq \varepsilon, & j = 1, \cdots, M, \quad j \neq k \\ 0 \leq \rho_e \leq 1, & \forall e \end{array} \tag{17}$$

where $\varepsilon \ll 1$ is a given very small value. As a bad choice of ε could imply a lack of solutions for the problem, we have here opted for a double-bound formulation that reformulates the optimization problem.

3.1 An alternative problem formulation

The concept of bound formulation dates back to Taylor and Bendsøe (1984) for reformulating min-max structural design problems. More recently, this concept has successfully been applied to avoid non-differentiability issues associated with mode switching when maximizing the difference between two consecutive eigenfrequencies (Jensen and Pedersen 2006). Under these considerations, the new formulation proposed is the following

$$\max_{\boldsymbol{\rho},\beta,\alpha} : \beta - \alpha \tag{18}$$

subject to

$$\begin{array}{ll} F_k(\boldsymbol{\rho}) \geq \beta & \\ |F_j(\boldsymbol{\rho})| \leq \alpha, & j = 1, \cdots, M, \quad j \neq k \\ 0 \leq \rho_e \leq 1, & \forall e \\ \beta, \alpha \geq 0 & \end{array} \tag{19}$$

where β and α are two extra non-negative variables in the optimization problem. In this way, we pretend to maximize the kth mode by forcing the coefficient F_k to stay over β, at the same time we reduce the rest of coefficients F_j as much as possible by introducing α.

Once the derivatives $\partial F_k / \partial \rho_e$ have been computed, the discrete problem is numerically solved by MMA (Svanberg 1987). In the next subsection, we explain how to carry out the sensitivity analysis.

3.2 Sensitivity analysis

Having in mind that

$$F_k(\boldsymbol{\rho}) = \mathbf{G}_k^T \mathbf{P}(\boldsymbol{\varphi}(\boldsymbol{\rho}), \overline{\|\nabla \hat{\boldsymbol{\varphi}}(\boldsymbol{\rho})\|_\delta}) \tag{20}$$

the main point here is to compute the derivative of the electrode profile $\mathbf{P}$ with respect to ρ_e. In this case

$$\frac{\partial \mathbf{P}}{\partial \rho_e} = \sum_{i=1}^{N_e} \left(\frac{\partial \mathbf{P}}{\partial \varphi_i} \frac{\partial \varphi_i}{\partial \rho_e} + \frac{\partial \mathbf{P}}{\partial \overline{\|\nabla \hat{\varphi}_i\|_\delta}} \frac{\partial \overline{\|\nabla \hat{\varphi}_i\|_\delta}}{\partial \rho_e} \right) \tag{21}$$

where $\partial \varphi_i / \partial \rho_e$ represents the standard modification of sensitivities due to smothering and projection. The second term can be expressed as

$$\frac{\partial \overline{\|\nabla \hat{\varphi}_i\|_\delta}}{\partial \rho_e} = \frac{\partial \overline{\|\nabla \hat{\varphi}_i\|_\delta}}{\partial \|\nabla \hat{\varphi}_i\|_\delta} \frac{\partial \|\nabla \hat{\varphi}_i\|_\delta}{\partial \|\nabla \hat{\varphi}_i\|} \frac{\partial \|\nabla \hat{\varphi}_i\|}{\partial \rho_e} \tag{22}$$

where the first contribution is due to the second projection, the second is just the scaling factor, δ, and the third one is computed as

$$\frac{\partial \|\nabla \hat{\varphi}_i\|}{\partial \rho_e} = \frac{1}{\|\nabla \hat{\varphi}_i\|} \left(\frac{\partial \hat{\varphi}_i}{\partial x} \frac{\partial}{\partial \rho_e} \left(\frac{\partial \hat{\varphi}_i}{\partial x} \right) + \frac{\partial \hat{\varphi}_i}{\partial y} \frac{\partial}{\partial \rho_e} \left(\frac{\partial \hat{\varphi}_i}{\partial y} \right) \right) \tag{23}$$

where

$$\frac{\partial}{\partial \rho_e} \left(\frac{\partial \hat{\varphi}_i}{\partial x} \right) = \frac{\partial}{\partial \varphi_k} \left(\frac{\partial \hat{\varphi}_i}{\partial x} \right) \frac{\partial \varphi_k}{\partial \rho_e} \tag{24}$$

being

$$\frac{\partial}{\partial \varphi_k} \left(\frac{\partial \hat{\varphi}_i}{\partial x} \right) = \mathbf{B}_x \mathbf{K}_{\mathbf{F}_2}^{-1} \mathbf{T}_\mathbf{F} \tag{25}$$

and

$$\frac{\partial \varphi_k}{\partial \rho_e} = \mathbf{T}_\mathbf{F}{}^T \mathbf{K}_{\mathbf{F}_1}^{-1} \mathbf{T}_\mathbf{F} \tag{26}$$

is again the sensitivity due to the first-step filtering (smoothing and projection). The calculation of these two terms, eq. (25) and (26) are described in detail in Clausen et al. (2015) and in Lazarov and Sigmund (2011), respectively. The term concerning y is obtained in a similar way, just replacing $\mathbf{B}_x$ by $\mathbf{B}_y$.

4 Numerical examples in 2d

This section is devoted to show numerical examples. Some of the parameters are the same for all of them. As we did in the 1d example, we will use unit side elements length, the threshold is $\eta_1 = \eta_2 = 0.5$, and the sharpness parameters are high in the beginning, $\beta_1 = \beta_2 = 8$, and both are gradually increased to 128 by doubling at every 50 iterations. The iterative process typically converges after 100 iterations (the starting point in each case is the solution corresponding to zero gap). We will just change the boundary conditions of the plate, the index k of the mode to be filtered, and the number of modes M to be considered. The flow chart of computations for the approach proposed is detailed in Fig. 6. Notice that as the host structure is fixed, the eigenmodes can be pre-computed and do not change during the optimization process.

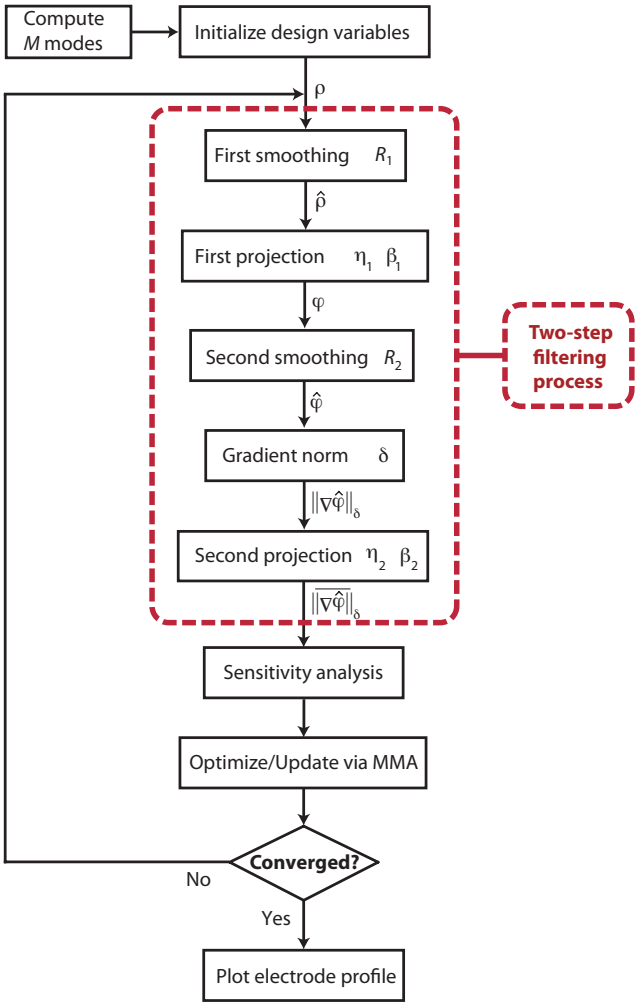

Fig. 6 Flowchart

4.1 Example 1: simply-supported plate

We start by considering a plate simply-supported at all four edges for which the 1st mode is isolated among the first $M = 10$ modes. We examine first the convergence when the mesh is refined. Due to symmetry, in Fig. 7 it is just shown a quarter of the electrode pattern of dimensions 50 by 50 with element side lengths of 1 (left) and 0.5 (right), respectively. The value of the filter radii are $R_1 = 16$, $R_2 = 10$. As it is observed, the gap-phase is quite uniform and practically independent of the discretization.

Now we analyze the dependence on the gap-width by varying the value of R_2 for a (fixed) mesh of 100 by 100 elements. It is observed in Fig. 8 that the gap is doubled when doubling the value of R_2 as well, and its width increases as expected.

For this example, the optimized design obtained with this formulation is practically identical to the one that corresponds to imposing a gap-phase of given width

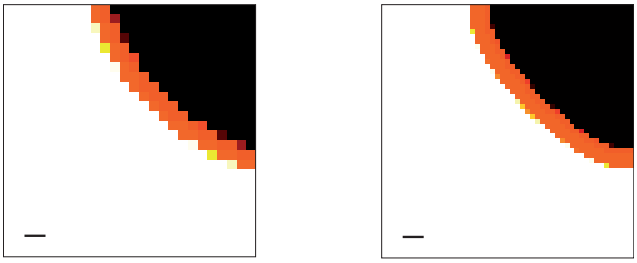

Fig. 7 Convergence on mesh size: (left) 50 × 50 elements; (right) 100 × 100 elements. The black bars represent the width w_{gap}.

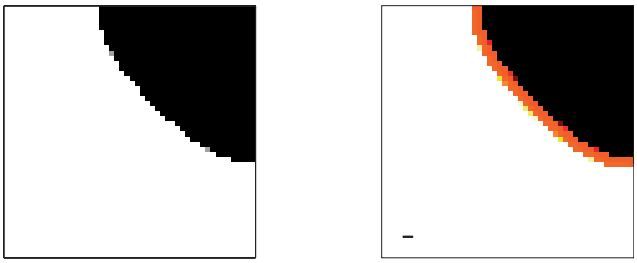

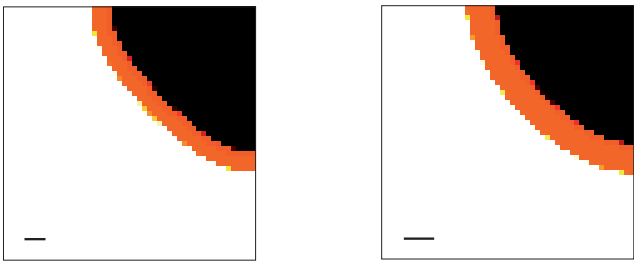

Fig. 8 Dependence on the gap-width: (left top) $w_{gap} = 0$; (right top) $R_2 = 5$, $w_{gap} = 2$; (left bottom) $R_2 = 10$, $w_{gap} = 4$; (right bottom) $R_2 = 15$, $w_{gap} = 6$.

over the structure with no gap, and that is the reason why the latter is not shown here. In the following this equality is disappearing.

4.2 Example 2: plate clamped at its both extreme sides

Now a rectangular plate clamped at both ends is considered, for which the 1st mode is isolated among the first $M = 14$ modes. The mesh used is 204 by 60 elements with unit side lengths, and $R_1 = 10$, $R_2 = 5$. Fig. 9 shows the optimal structure with the gap-phase (now in gray) imposed at a later stage (top) and the one obtained with the formulation that includes the gap-phase in orange (below). Both are very similar, but some differences can be observed in the areas inside the circle (and in others, due to symmetry).

In order to see how sensitive the structure is to the gap, Fig. 10 shows the normalized response of the first

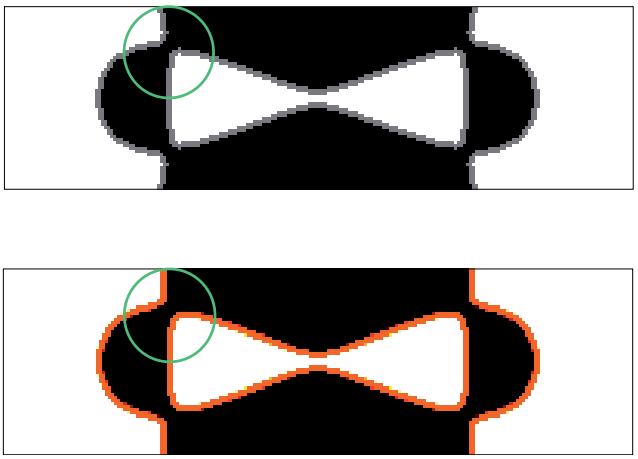

Fig. 9 Electrode pattern that isolates the 1st mode among the first 14 modes in a plate clamped at its both extreme sides; (top) the gap is imposed a posteriori; (below) the gap is considered in the formulation. Green circle represents where small differences occur between the designs.

14 modes. The normalization consists in dividing all coefficients F_k by the coefficient F_1 because the 1st mode is precisely the maximized one among the rest. Three cases are represented: in blue the response of the design with no gap; in grey the response when the gap is imposed after optimization, and in orange when the gap is included in the optimization problem. We can mainly observe two things: first, some modes appear upon introducing a gap-phase, and second, although we have used a logarithmic scale to represent the values, this influence is significantly lower (three orders of magnitude in this example) when including the gap design in the formulation.

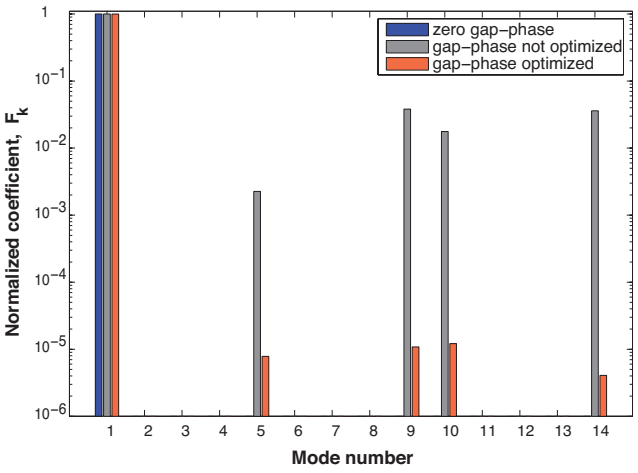

Fig. 10 Normalized amplitude for the first 14 modes (refer to Fig. 9)

Fig. 11 shows the previous example with a new requirement, an outside frame of gap-phase of same width as the one enforced inside. As explained before, an easy way to do that is to use a passive area along the domain boundaries with half the gap width of that imposed in the interior. Nodes inside the passive area are excluded from the filter, and nodes at the interface between the passive area and the active part of the domain are restricted to 1/2. Despite both designs showing quite similar layouts, it is pointed out in Fig. 12 that small variations in the geometry, imply once more really significative changes in the response of the other coefficients. The optimization cancels the influence of the rest of the modes!

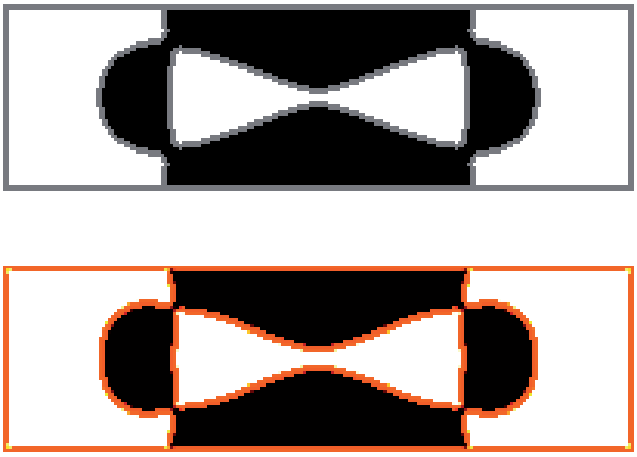

Fig. 11 Same example as before; (top) the gap is imposed a posteriori; (below) the inside gap is considered in the formulation and half of the outside gap is imposed as a passive area.

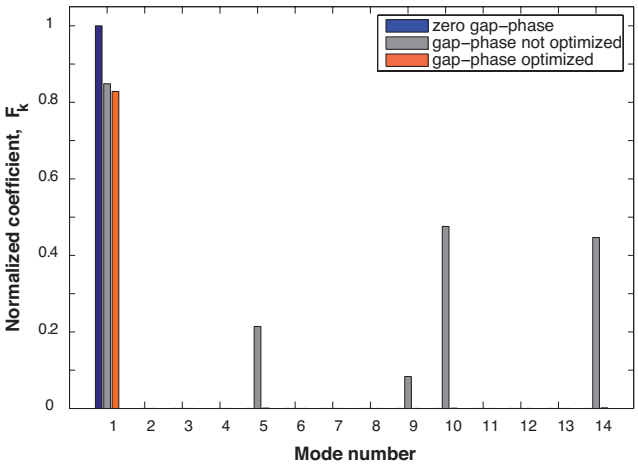

Fig. 12 Normalized amplitude for the first 14 modes (refer to Fig. 11)

In the final example some mayor changes become visible in the geometry upon introducing the gap-phase.

4.3 Example 3: plate fixed at its left side

The last example considered is a plate fixed at its left side. Now we are interested in isolating the sixth mode among the first twenty modes. In contrast to the previous examples, the gap-phase is placed in a different way than when it is imposed a posteriori (see Fig. 13). This directly influences the normalized response (as before, the coefficients F_k are divided by F_6 corresponding to zero gap). As can be observed in Fig. 14, though we "awake" other modes (in orange) more than when the gap-phase is not optimized (in gray), the amplitude for the 6th mode is increased much more, showing finally a gain, expressed as $(\beta-\alpha)_{gap\ opt}$, of 33% compared to imposing the gap at a later stage, $(\beta-\alpha)_{gap}$.

Fig. 13 Electrode pattern that isolates the 6th mode among the first 20 modes in a plate fixed at its left side; (left) the gap is imposed a posteriori; (right) the gap is considered in the formulation.

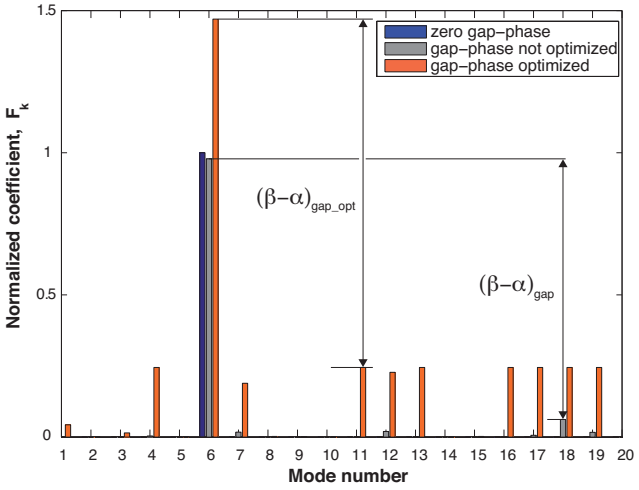

Fig. 14 Normalized amplitude for the first 20 modes

The fact that the design in Fig. 13 (right) shows a different topology compared to Fig. 13 (left) is simply

due to the formulation, more specifically, to β. If we take normalized coefficients such that $\beta < 1$, the final design including gap (see Fig. 15 (right)) shows now the same topology. In this case, the design shown in Fig. 15 (left) - a copy of Fig. 13 (left) - is virtually non-sensitive to the rest of the modes judging from Fig. 14. Consequently the design in Fig. 15 (right) is hardly better than design in Fig. 15 (left) and that is the reason why its normalized response has not been included in Fig. 14.

Fig. 15 Same example as before; (left) a copy of Fig. 13 (left); (right) the gap is considered in the formulation when $\beta < 1$.

5 Conclusions

In this work, a systematic procedure that introduces a uniform null-polarity phase (gap-phase) of known width between areas of opposite polarity on designing piezoelectric modal transducers is developed. Although in some cases the electrode profiles are quite similar to the ones corresponding to imposing the gap at a later stage, in other cases the designs are quite different, and when they are not, it is shown how small variations can lead to significative changes in the response. It is worthwhile to emphasize that the approach developed here, in the context of piezo modal filters, is also valid for other piezoelectric devices since practise always requires a small separation between phases of opposite polarity to avoid short-circuits. This technique may be combined with the robust approach (Wang. et al 2011) to control feature size of both black and white phases as well.

Acknowledgements The major part of this work was performed while AD was visiting the Department of Mechanical Engineering, DTU, Lyngby. The stay was supported by a fellowship of UCLM (Spain). The work has also been supported by the Ministerio de Economía y Competitividad through grant MTM2013-47053-P, (Spain, AD), and from the Villum Foundation through the NextTop project (Denmark, OS). The authors acknowledge stimulating discussions on the subject of this paper with Anders Clausen, Erik Andreassen, José Carlos Bellido and José Luis Sánchez-Rojas.

References

Andreassen E, Clausen A, Schevenels M, Lazarov BS, Simgund O (2011) Efficient topology optimization in MATLAB using 88 lines of code. Struct Multidisc Optim 43:1-16

Bendsøe MP, Sigmund O (1999) Material interpolation schemes in topology optimization. Arch Appl Mech 69:635-654

Donoso A, Bellido JC (2009a) Systematic design of distributed piezoelectric modal sensors/actuators for rectangular plates by optimizing the polarization profile. Struct Multidisc Optim 38:347-356

Donoso A, Bellido JC (2009b) Tailoring distributed modal sensors for in-plane modal filtering. Smart Mater Struct 18:037002

Donoso A, Bellido JC, Chacón JM (2010) Numerical and analytical method for the design of piezoelectric modal sensors/actuators for shell-type structures. Int J Numer Meth Engng 81:1700-1712

Clausen A, Aage N, Sigmund O (2015) Topology optimization of coated structures and material interface problems. Comput Methods Appl Mech Engrg 209: 524-541

Carbonari RC, Silva ECN, Nishiwaki S (2007) Optimal placement of piezoelectric material in piezoactuator design, Smart Mater Struct 16:207-220

Guest J, Prevost J, Belytschko T (2004) Achieving minimum length scale in topology optimization using nodal design variables and projection functions. Int J Numer Meth Engng 61 (2): 238–254

Jensen JS, Pedersen NL (2006) On maximal eigenfrequency separation in two-material structures: the 1D and 2D scalar cases. J Sound Vib 289:967-986

Jian K, Friswell MI (2007) Distributed modal sensors for rectangular plate structures. J Intell Mater Syst Struct 18:939-948

Kang Z, Wang X, Luo Z (2012) Topology optimization for static control of piezoelectric plates with penalization on intermediate actuation voltage. Journal of Mechanical Design 134:051006

Kim J, Hwang JS, Kim SJ (2001) Design of modal transducers by optimizing spatial distribution of discrete gain weights. AIAA Journal 39(10):1969–1976

Kögl M, Silva ECN (2005) Topology optimization of smart structures: design of piezoelectric plate and shell actuators. Smart Mater Struct 14:387–399

Kucera M, Manzaneque T, Sánchez-Rojas JL, Bittner, Schmid U (2013) Q-factor enhancement for self-actuated self-sensing piezoelectric MEMS resonators applying a lock-in driven feedback loop. J Micromech Microeng 23:085009

Lazarov BS, Sigmund O (2011) Filters in topology

optimization as a solution to Helmholtz type differential equation. Int J Numer Methods Eng 86(6):765–781

Lee CK, Moon FC (1990) Modal sensors/actuators. J Appl Mech 57:434–441

Luo Z, Gao W, Song C (2010) Design of multi-phase piezoelectric actuators. Journal of Intelligent Material Systems and Structures 21:1851-1865

Preumont A, Francois A, De Man P, Piefort V (2003) Spatial filters in structural control. J Sound Vib 265(1): 61–79

Pulskamp JS, Bedair SS, Polcawich RG, Smith GL, Martin J, Power B, Bhave SA (2012) Electrode-shaping for the excitation and detection of permitted arbitrary modes in arbitrary geometries in piezoelectric resonators. IEEE Transactions on ultrasonics, ferroelectrics, and frequency control 59(5):1043-1060

Sánchez-Rojas JL, Hernando J, Donoso A, Bellido JC, Manzaneque T, Ababneh A, Seidel H, Schmid U(2010) Modal optimization and filtering in piezoelectric microplate resonators. J Micromech Microeng 20:055027

Sigmund O (2007) Morphology-based black and white filters for topology optimization. Struct Multidisc Optim 33 (4-5): 401-424

Silva ECN, Kikuchi N (1999) Design of piezoelectric transducers using topology optimization. Smart Mater Struct 8:350-364

Sun D, Tong L, Wang D (2002) Modal actuator/sensor by modulating thickness of piezoelectric layers for smart plates. AIAA Journal 40(8):1676–1679

Svanberg K (1987) The method of moving asymptotes - a new method for structural optimization. Int J Numer Methods Eng 24:359-373

Taylor JE, Bendsøe MP (1984) An interpretation for min-max structural design problems including a method for relaxing constraints. Int J Solids Structures 20(4):301-314

Wang F, Lazarov B, Sigmund O (2011) On projection methods, convergence and robust formulations in topology optimization. Struct Multidisc Optim 43:767-784

Zhang X, Kang Z, Li M (2014) Topology optimization of electrode coverage of piezoelectric thin-walled structures with CGVF control for minimizing sound radiation. Struct Multidisc Optim 50:799-814